ORIGINAL ARTICLE

lajss.org
Latin American Journal of Solids and Structures

www.lajss.org

Study on the structural damage detection method using the flexibility matrix

Muyu Zhang[a,b*], Xiaoyang Peng[a], Yujia Li[a], Ziping Wang[a,c], Jianguo Zhu[a,b], Jian Zhang[a,b,d]

[a]Faculty of Civil Engineering and Mechanics, Jiangsu University, Zhenjiang 212013, China. E-mails: muyu@ujs.edu.cn, 2531862106@qq.com, 1242467482@qq.com, wzp@ujs.edu.cn, zhujg@ujs.edu.cn, jianzhang@ujs.edu.cn
[b]National Center for International Research on Structural Health Management of Critical Components, Faculty of Civil Engineering and Mechanics, Jiangsu University, Zhenjiang 212013, China. E-mails: muyu@ujs.edu.cn, zhujg@ujs.edu.cn, jianzhang@ujs.edu.cn
[c]Department of Aeronautics, Polytechnic University of Madrid, Madrid 28040, Spain. E-mails: wzp@ujs.edu.cn
[d]Ocean Institute, Northwestern Polytechnical University, Taicang 215400, China. E-mails: jianzhang@ujs.edu.cn

* Corresponding author: Muyu Zhang. Email: muyu@ujs.edu.cn

https://doi.org/10.1590/1679-78257966

Abstract

The flexibility matrix finds extensive application in detecting damage in civil and mechanical engineering structures, a focus explored in-depth within this paper. This study meticulously examines distinct components of the flexibility matrix, namely the proposed Diagonal of the Flexibility Matrix Vector (DFV) and a singular row/column of the flexibility matrix (RFV). Both DFV and RFV can be represented uniquely as a specialized form-a weighted combination of the Hadamard product of two mode shapes. Sensitivity analysis reveals that DFV undergoes a sharp change in proximity to damage, establishing it as a dependable indicator for pinpointing damage locations. Conversely, this characteristic is not consistently observed with RFV. The results of numerical simulations conducted on a 16-story frame structure corroborate the outcomes of the sensitivity analysis, underscoring the efficacy of DFV not only in localizing damage but also in gauging its severity. To illustrate the potential and limitations of DFV/RFV in practical scenarios, damage localization for the I-40 Bridge is provided.

Keywords

Damage detection; Damage localization; Flexibility; Sensitivity;

Graphical Abstract

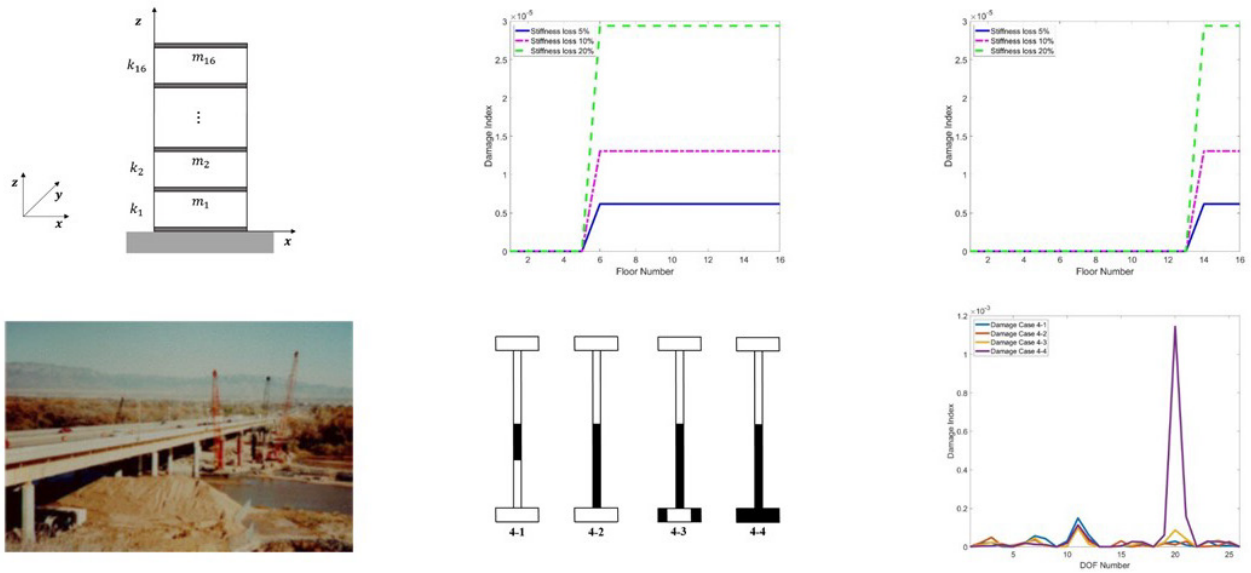

Received: December 12, 2023. In revised form: April 09, 2024. Accepted: May 06, 2024. Available online: May 17, 2024
https://doi.org/10.1590/1679-78257966

1 INTRODUCTION

Structural Health Monitoring (SHM) is of great importance for ensuring the security and integrity of the engineering structures (De Menezes et al. 2021; Zhang et al. 2022). It has received considerable attention from researchers and engineers worldwide (Avci et al. 2021). One of the key issues of SHM is to detect, locate and evaluate the damage before it affects the performance of the structure. Over the past few decades, various techniques have been adopted in the field of damage detection, which can be categorized into different types, including global/local, static/dynamic, or time/time-frequency/frequency (Gharehbaghi et al. 2022).

The vibration-based damage detection method belongs to the global and dynamic category, which is easy to conduct in real structure that can be dated back to 1960s (Sohn et al. 2003). The basic idea of vibration-based damage detection is that: As long as the physical properties of the structure changes because of the occurrence of the damage, the dynamic properties of the structure will also change. Using the change of this dynamic property, the damage can be detected (De Medeiros et al. 2018). Therefore, the dynamic property that can imply the damage is the key for structural damage detection.

Many kinds of the dynamic property have already been used for damage detection, such as frequency (Kim et al. 2003; De Medeiros et al. 2016), mode shape (Messina et al. 1998), damping (Mustafa et al. 2018), flexibility matrix (Pandey and Biswas 1995), frequency response function (Sartorato et al. 2017; Marques et al. 2018), correlation function (Wang et al. 2010; Zhang et al. 2023), transmissibility (Maia et al. 2011) and so on. Different dynamic property has its own advantages and disadvantages that could not solve all kinds of problems encounter in real application. For example, the frequency is very easy to obtain compare to the mode shape and damping ratio. It is a good indicator for the damage existence, while it is always very difficult to locate the damage when use it alone. Zhao and DeWolf (1999) employed sensitivity analysis to show the flexibility is more sensitive to damage than either frequency or mode shape. The flexibility matrix, which is considered as the inverse of the stiffness matrix, can be obtained using just a few lower orders of the modal parameters. High order modal parameters that hard to get will contribute very limit to build the flexibility matrix. This merit attracts lots of the researchers to build the damage index based on the flexibility matrix to detect the damage as early as 1990s.

Pandey and Biswas (1995) used the largest element in each column of flexibility matrix difference before and after damage to locate the cut in a steel beam. Ko et al. (2002) proposed a multi-stage scheme based on the diagonal of the flexibility matrix to detect the damage for a bridge. Zhang and Aktan (1995) proposed flexibility curvature index which only needs current information of the structure to determine the structural state. Wu and Law (2005) found that while considering truncation error, incomplete measurement and noise, the Uniform Load Surface (ULS) curvature is feasible for damage detection of the plane structure. Based on the ULS, Wang and Qiao (2007) and Qiao et al. (2007) developed three damage detection algorithms for beam-type and composite laminated plane structure: generalized fractal dimension (GFD), simplified gapped-smoothing (SGS) and strain energy method (SEM). Jung et al. (2015) proposed a normalized ULS (NULS) for beam-type structure, which show lower false positive and false negative rate than ULS. Zhang et al. (2013) applied ULS in a frame structure of IASC-ASCE, without the requirement of the structural mass information. Liu et al (2021) introduced a method for damage detection employing a generalized flexibility matrix constructed from incomplete modal data. Bernagozzi et al. (2022) tested the applicability of the flexibility-based damage detection method on the full-scale reinforce concrete building that experienced earthquake-induced damage. Sun et al. (2022) used a multiple-stage dynamic flexibility analysis that can be used for damage assessment for 27-bar truss structure and a steel frame structure numerically and experimentally. By comparison to other flexibility-based methods, this method has a better anti-noise ability and a higher calculation accuracy.

Besides, some researchers used the decomposition of the flexibility matrix for damage detection. Bernal (2002) designed a set of damage locating vectors (DLVs) obtained from the singular value decomposition of the difference of flexibility matrix. Apply DLVs in a structure, the zero stress fields will appear in the damage location, which can be used to identify the damage. Gao et al. (2004) applied DLV to a truss structure with ambient vibration with noise and verified it experimentally. Duan et al. (2005) introduced a proportional flexibility matrix for damage detection in ambient vibration based on DLV shows good results. An et al. (2017) introduced a rank-revealing QR decomposition technique to propose a rank-revealing QR decomposition based DLV (RRQR-DLV), which is higher sensitive than stochastic DLV.

Furthermore, the flexibility matrix is combined with other techniques for damage detection. Jaishi and Ren (2006) presented a combination of structural flexibility with modal updating technique, which is feasible for damage detection with 3% noise. Katebi et al. (2018) developed a structural-flexibility- sensitivity-based modal updating method, considering effort of mass modeling error and measurement error. Example of truss and frame shows good performance for identify the damage location and quantify the damage severity. Entezami et al. (2020) applied the difference of structural flexibility as the damage-sensitive feature, combined with the *k*-medoids and density-based spatial clustering, correctly identified the damage of the ASCE benchmark shear frame. Yang and Huang (2021) made flexibility diagonal curvature as the input of convolutional neutral network and apply in a three-span concrete girder bridge, which can

identify the damage location and damage extent correctly. Dinh-Cong et al. (2023) found even the mode shape data is polluted by 10% noise, the flexibility-sensitivity-based damage index can still be used for the damage assessment of functionally graded beams.

In summary, from these studies different part of the flexibility matrix is used for different kind of structure with promising results. But there still lies a question that why these proposed damage index can be used for damage detection and what is the restrictions that these methods can be used. In this paper, different part of the flexibility matrix, the diagonal and one row/column, is expressed in a special form that the inherent mechanism of its ability for damage localization is revealed using the sensitivity analysis. Firstly, the vector DFV/RFV that using the diagonal and one row/column of the flexibility matrix is established based on the vibration theory. Sensitivity analysis of these two vectors to the local stiffness show their potential for damage localization. Then, damage detection of a 16-story shear frame verifies the sensitivity analysis results and show the detectability of these two vectors. Finally, real structural application of I-40 Bridge is used to show the effectiveness and the restrictions of the DFV/RFV.

2 THEORY

2.1 Establishment of damage index

The structural flexibility matrix $\boldsymbol{F}$ can be represented as a synthesis of both frequencies and mode shapes

$$\boldsymbol{F}=\sum_{i=1}^{n}\frac{1}{\left(\omega_n^j\right)^2}\boldsymbol{\Phi}_i\boldsymbol{\Phi}_i^T=\sum_{i=1}^{n}\frac{1}{\left(\omega_n^j\right)^2}\begin{bmatrix}\phi_{1i}\\ \phi_{2i}\\ \vdots\\ \phi_{ni}\end{bmatrix}\begin{bmatrix}\phi_{1i} & \phi_{2i} & \cdots & \phi_{ni}\end{bmatrix}=\sum_{i=1}^{n}\frac{1}{\left(\omega_n^j\right)^2}\begin{bmatrix}\phi_{1i}\phi_{1i} & \phi_{1i}\phi_{2i} & \cdots & \phi_{1i}\phi_{ni}\\ \phi_{2i}\phi_{1i} & \phi_{2i}\phi_{2i} & \cdots & \phi_{2i}\phi_{ni}\\ \vdots & \vdots & \ddots & \vdots\\ \phi_{ni}\phi_{1i} & \phi_{ni}\phi_{2i} & \cdots & \phi_{ni}\phi_{ni}\end{bmatrix} \tag{1}$$

where ω_n^i is the i^{th} natural frequency and ϕ_{ji} is the j^{th} element of the i^{th} mode shape $\boldsymbol{\Phi}_i$.

Hence, a specialized representation can be employed to express a vector comprising the diagonal elements of the flexibility matrix, referred to as the Diagonal of the Flexibility Matrix Vector (DFV).

$$\boldsymbol{D}_F=diag(\boldsymbol{F})=\sum_{i=1}^{n}\frac{1}{\left(\omega_n^i\right)^2}[\phi_{1i}\phi_{1i},\quad \phi_{2i}\phi_{2i},\quad \cdots,\quad \phi_{mi}\phi_{mi}]^T=\sum_{i=1}^{n}\frac{1}{\left(\omega_n^i\right)^2}\boldsymbol{\Phi}_i\circ\boldsymbol{\Phi}_i \tag{2}$$

where '$\circ$' is the Hadamard product (Styan 1973).

Similarly, one can express the r^{th} row or column of the flexibility matrix (RFV) in the following form

$$\boldsymbol{R}_F^r=\sum_{i=1}^{n}\frac{1}{\left(\omega_n^i\right)^2}[\phi_{1i}\phi_{ri},\quad \phi_{2i}\phi_{ri},\quad \cdots,\quad \phi_{ni}\phi_{ri}]^T=\sum_{i=1}^{n}\frac{1}{\left(\omega_n^i\right)^2}\boldsymbol{\Phi}_r\circ\boldsymbol{\Phi}_i \tag{3}$$

Subsequently, the damage indices based on flexibility can be defined as the absolute difference in DFV/RFV values before and after the occurrence of damage.

$$\boldsymbol{DI}=\left|\boldsymbol{S}^d-\boldsymbol{S}^u\right| \tag{4}$$

where $\boldsymbol{S}^d$ and $\boldsymbol{S}^u$ is the damaged and undamaged DFV $\boldsymbol{D}_F$ or RFV $\boldsymbol{R}_F^r$, respectively.

2.2 Sensitivity analysis

In order to study this DFV/RFV-based damage index, sensitivity analysis is used. Sensitivity of a variable y to x is expressed as

$$\eta(y/x)=\lim_{\Delta x\to 0}(\frac{\Delta y}{y})/(\frac{\Delta x}{x})=\frac{x}{y}\frac{\partial y}{\partial x} \tag{5}$$

which reflects the change of variable y when x changes.

Using this definition, the sensitivity of DFV to the local stiffness k_j, $\eta\left(D_F/k_j\right)$, is expressed by

$$\eta(\boldsymbol{D}_F / k_j)\circ\boldsymbol{D}_F = k_j\frac{\partial \boldsymbol{D}_F}{\partial k_j} = k_j\frac{\partial}{\partial k_j}[\sum\nolimits_{i=1}^{n}\frac{1}{\left(\omega_n^i\right)^2}\boldsymbol{\Phi}_i\circ\boldsymbol{\Phi}_i]$$
$$= k_j\sum\nolimits_{i=1}^{n}\left\{\frac{\partial}{\partial k_j}\left[\frac{1}{\left(\omega_n^i\right)^2}\right]\boldsymbol{\Phi}_i\circ\boldsymbol{\Phi}_i + \frac{1}{\left(\omega_n^i\right)^2}\frac{\partial}{\partial k_j}\left(\boldsymbol{\Phi}_i\circ\boldsymbol{\Phi}_i\right)\right\} \tag{6}$$

Considering that, based on the definition of sensitivity

$$\eta([\frac{1}{\left(\omega_n^i\right)^2}]/k_j) = k_j(\omega_n^i)^2\frac{\partial}{\partial k_j}[\frac{1}{\left(\omega_n^i\right)^2}] \tag{7}$$

$$\eta((\boldsymbol{\Phi}_i\circ\boldsymbol{\Phi}_i)/k_j)\circ\boldsymbol{\Phi}_i\circ\boldsymbol{\Phi}_i = k_j\frac{\partial}{\partial k_j}(\boldsymbol{\Phi}_i\circ\boldsymbol{\Phi}_i) \tag{8}$$

Eq. (6) can be written as

$$\eta(\boldsymbol{D}_F / k_j)\circ\boldsymbol{D}_F = \sum\nolimits_{i=1}^{n}\frac{1}{\left(\omega_n^i\right)^2}\boldsymbol{\Phi}_i\circ\boldsymbol{\Phi}_i\circ\left\{\eta\left(\left[\frac{1}{\left(\omega_n^i\right)^2}\right]/k_j\right)[1]_{n\times1} + \eta(\left(\boldsymbol{\Phi}_i\circ\boldsymbol{\Phi}_i\right)/k_j)\right\} \tag{9}$$

Using the characteristic of the sensitivity, Eq. (9) can be further expressed as

$$\eta(\boldsymbol{D}_F / k_j) = \boldsymbol{D}_F^{\circ(-1)}\sum\nolimits_{i=1}^{n}\frac{1}{\left(\omega_n^i\right)^2}\boldsymbol{\Phi}_i\circ\boldsymbol{\Phi}_i\circ\{-2\eta(\omega_n^i / k_j)[1]_{n\times1} + 2\eta(\boldsymbol{\Phi}_i / k_j)\} \tag{10}$$

where $\boldsymbol{D}_F^{\circ(-1)}$ is the Hadamard inverse (Reams 1999) of $\boldsymbol{D}_F$, $\eta\left(\omega_n^i/k_j\right)$ is the sensitivity of i^{th} frequency ω_n^i to the local stiffness k_j, expressed as

$$\eta(\omega_n^i / k_j) = \frac{k_j}{\omega_n^i}\frac{\partial\omega_n^i}{\partial k_j} \tag{11}$$

and $\eta\left(\boldsymbol{\Phi}_i/k_j\right)$ is the sensitivity of i^{th} mode shape $\boldsymbol{\Phi}_i$ to the local stiffness k_j, expressed as

$$\eta(\boldsymbol{\Phi}_i / k_j) = [\eta(\phi_{1i} / k_j),\quad \eta(\phi_{2i} / k_j),\quad \cdots,\quad \eta(\phi_{ni} / k_j)]^T \tag{12}$$

where

$$\eta(\phi_{si} / k_j) = \frac{k_j}{\phi_{si}}\frac{\partial\phi_{si}}{\partial k_j} \tag{13}$$

Similarly, the sensitivity of RFV to the local stiffness k_j, $\eta\left(\boldsymbol{R}_F^r/k_j\right)$is expressed by

$$\eta\left(\boldsymbol{R}_F^r / k_j\right) = \boldsymbol{R}_F^{r\circ(-1)}i = \sum\nolimits_{i=1}^{n}\frac{1}{\left(\omega_n^i\right)^2}\boldsymbol{\Phi}_r\circ\boldsymbol{\Phi}_i\circ\left\{-2\eta\left(\omega_n^i / k_j\right)[1]_{n\times1} + \eta\left(\boldsymbol{\Phi}_r / k_j\right) + \eta\left(\boldsymbol{\Phi}_i / k_j\right)\right\} \tag{14}$$

As a result, the sensitivity of the DFV/RFV to the local stiffness can be obtained by the sensitivity of mode parameters (frequency and mode shape) to the local stiffness.

From Eq. (10) and Eq. (11), the sensitivity of frequency and mode shape to the local stiffness is relate to the partial derivative of mode parameters to the local stiffness. If we assume the mass will not change as the stiffness changes when damage occurs, the expression for the partial derivative of frequency ω_n^i and mode shapes $\boldsymbol{\Phi}_i$ with respect to local stiffness k_j can be formulated as follows (Zhao and DeWolf 1999).

$$\frac{\partial \omega_n^i}{\partial k_j} = \frac{1}{2\omega_n^i} \boldsymbol{\Phi}_i^T \frac{\partial K}{\partial k_j} \boldsymbol{\Phi}_i \tag{15}$$

$$\frac{\partial \boldsymbol{\Phi}_i}{\partial k_j} = \Sigma_{L=1}^{N} \alpha_L \boldsymbol{\Phi}_L \tag{16}$$

where

$$\alpha_s = \begin{cases} \dfrac{1}{\left(\omega_n^i\right)^2 - \left(\omega_n^s\right)^2} \boldsymbol{\Phi}_s^T \dfrac{\partial \boldsymbol{K}}{\partial k} \boldsymbol{\Phi}_i & (i \neq s) \\ 0 & (i = s) \end{cases} \tag{17}$$

that the partial derivative of mode parameters to the local stiffness is related to the partial derivative of the stiffness matrix to the local stiffness.

According to the definition, the sensitivity $\eta\left(\boldsymbol{D}_F / k_j\right)$ in Eq. (10) reflects how the vector $\boldsymbol{D}_F$ changes when there is a variation in local stiffness. Considering the definition of the damage index $\boldsymbol{DI}$ in Eq. (4), the change of $\boldsymbol{D}_F$ is the damage index $\boldsymbol{DI}$ defined in this paper. As a result, the sensitivity of $\boldsymbol{D}_F$ to local stiffness $\eta\left(\boldsymbol{D}_F / k_j\right)$ reflects the shape of damage index $\boldsymbol{DI}$ as the local stiffness k_j changes.

3 NUMERICAL SIMULATION

3.1 Model description

Illustrated in Figure 1 is a 16-story shear frame structure. Each floor is characterized by a mass of 1.254 kg, and the local stiffness of the braces is 8505 N/m. Due to the significant disparity in structural stiffness between the y and x directions, the analysis focuses exclusively on motion in the x direction. The mass matrix and stiffness matrix for the frame structure are formulated as follows:

$$\boldsymbol{M} = \begin{bmatrix} m_1 & \cdots & 0 \\ \vdots & \ddots & \vdots \\ 0 & \cdots & m_{16} \end{bmatrix} \tag{18}$$

$$\boldsymbol{K} = \begin{bmatrix} k_1 + k_2 & -k_2 & & & \\ -k_2 & k_2 + k_3 & -k_3 & & \\ & \ddots & \ddots & \ddots & \\ & -k_{15} & & k_{15} + k_{16} & -k_{16} \\ & & & -k_{16} & k_{16} \end{bmatrix} \tag{19}$$

Following this, the calculation of the partial derivative of the stiffness matrix concerning local stiffness can be obtaind as

$$\frac{\partial \boldsymbol{K}}{\partial k_j}=\begin{bmatrix} \ddots & & & \\ & 1 & -1 & \\ & -1 & 1 & \\ & & & \ddots \end{bmatrix} \tag{20}$$

where value '1' is in $(j-1)^{th}$ row, $(j-1)^{th}$ column and j^{th} row, j^{th} column, and value '-1' is in $(j-1)^{th}$ row, j^{th} column and j^{th} row, $(j-1)^{th}$ column.

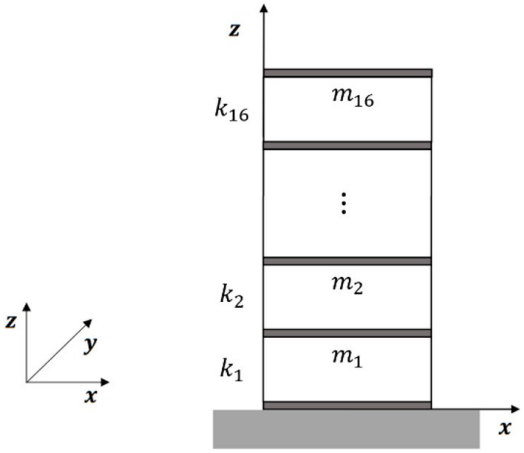

Figure 1 A 16-story shear frame structure.

3.2 Sensitivity analysis

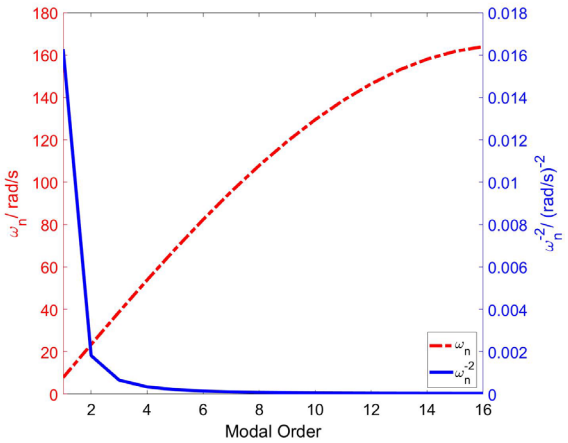

Figure 2 Change of the frequency with the modal order.

As in vibration theory, when the modal order increases, the frequency ω_n will also increase. Figure 2 is an example of the increase of the value ω_n when the modal order increases for the 16-story shear frame structure in Section 3.1. Look into the expression of the sensitivity of $\boldsymbol{D}_F$ to the local stiffness $\eta(\boldsymbol{D}_F/k_j)$ expressed in Eq. (10), the frequency ω_n is in the denominator. Hence, the value of $\eta(\boldsymbol{D}_F/k_j)$ is primarily influenced by the parameters related to the lower modal orders, as the value of $(\omega_n^i)^{-2}$ decreases very fast when the modal order increase which is also shown in Figure 2 for the case for the 16-story shear frame structure.

Besides, look into Eq. (10), as $\eta(\omega_n^i/k_j)$ is a constant value that will not affect the trend of $\eta(\boldsymbol{D}_F/k_j)$. The trend of $\eta(\boldsymbol{D}_F/k_j)$ will largely affected by the trend of the lower modal order value of $\eta(\boldsymbol{\Phi}_1/k_j)$. Figure 3 is the value of $\eta(\boldsymbol{\Phi}_1/k_j)$ for the case of 16-story frame structure. As shown in the figure, there is a sharp change of the value $\eta(\boldsymbol{\Phi}_1/k_j)$ near the stiffness change location, measurement point j, which implies the value $\eta(\boldsymbol{D}_F/k_j)$ will also have a sharp change near the stiffness change location. As illustrated in the figure, a pronounced shift in the value of $\eta(\boldsymbol{\Phi}_1/k_j)$ is evident in the vicinity of the stiffness change location, denoted as measurement point j. This suggests a corresponding sharp variation in the value of $\eta(\boldsymbol{D}_F/k_j)$ near the location of stiffness alteration.

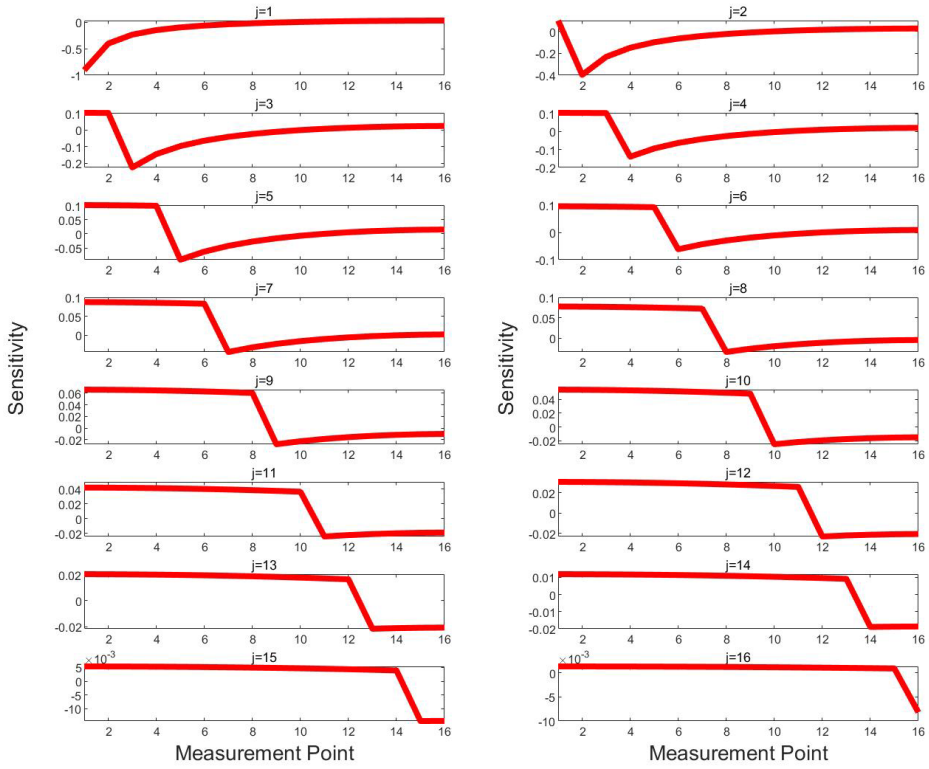

Figure 3 Sensitivity of the 1st mode shape to the local stiffness k_j, j=1-16.

Figure 4 shows the sensitivity analysis results of $\boldsymbol{D}_F$ to the local stiffness k_j at measurement points 1-16 of the 16-story shear frame structure. From Figure 4, a same phenomenon can be observed that $\eta(\boldsymbol{D}_F/k_i)$ has a sharp change around the stiffness change location, the measurement point j. This implies that in the presence of damage near measurement point j, the change of $\boldsymbol{D}_F$, as the damage index $\boldsymbol{DI}$ defined in Eq. (4), will also have a sharp change near the damage location. As a result, the sudden change of the DFV-based $\boldsymbol{DI}$ indicates the damage location. This DFV has a property feasible for the identification of damage.

On the other hand, Figure 5 is the sensitivity of 1st row/column $\boldsymbol{R}_F^1$ (red solid line) and 4th row/column $\boldsymbol{R}_F^4$ (green dash line) of the flexibility matrix to the local stiffness k_j from measurement point 1-16. As can be seen from the red line in Figure 5, the sensitivity analysis results are close to the results in Figure 4, that it also has a sharp change around the damage location, this is because in the expression of of $\eta\left(\boldsymbol{R}_F^1/k_j\right)$

$$\eta(\boldsymbol{R}_F^1 / k_j) = \boldsymbol{R}_F^{1\circ(-1)} \sum_{i=1}^{n} \frac{1}{\left(\omega_n^i\right)^2} \boldsymbol{\Phi}_1 \circ \boldsymbol{\Phi}_i \circ (-2\eta(\omega_n^i / k_j)[1]_{n\times 1} + \eta(\boldsymbol{\Phi}_1 / k_j) + \eta(\boldsymbol{\Phi}_i / k_j)\} \tag{21}$$

$\eta\left(\boldsymbol{\Phi}_1/k_j\right)$ still play an important part to determine the trend of $\eta\left(\boldsymbol{R}_F^1/k_j\right)$. Therefore, the 1st row/column of the flexibility matrix still can be used for damage detection. While for the green line in Figure 5, the results are random, this is because in the expression of $\eta\left(\boldsymbol{R}_F^4/k_j\right)$

$$\eta(\boldsymbol{R}_F^4 / k_j) = \boldsymbol{R}_F^{4\circ(-1)} \sum_{i=1}^{n} \frac{1}{\left(\omega_n^i\right)^2} \boldsymbol{\Phi}_4 \circ \boldsymbol{\Phi}_i \circ (-2\eta(\omega_n^i / k_j)[1]_{n\times 1} + \eta(\boldsymbol{\Phi}_4 / k_j) + \eta(\boldsymbol{\Phi}_i / k_j)\} \tag{22}$$

$\eta\left(\boldsymbol{\Phi}_4/k_j\right)$ plays an important part to determine the trend of $\eta\left(\boldsymbol{R}_F^4/k_j\right)$. While the 4th mode shape $\boldsymbol{\Phi}_4$ is not sensitive to the damage location, it pollutes the trend from low order $\eta\left(\boldsymbol{\Phi}_i/k_j\right)$ that makes $\eta\left(\boldsymbol{R}_F^4/k_j\right)$ do not have the sudden change around the damage location, which means the 4th row/column of the flexibility matrix couldn't be used for damage detection.

In summary, as we know the damage only effect a few mode shapes. This DFV-based method works for the lower mode shape that is sensitive to the damage. While for the RFV-based method, although there is the term $\eta\left(\boldsymbol{\Phi}_r/k_j\right)$ in the expression, even this mode shape $\boldsymbol{\Phi}_r$ is sensitive to the damage location, the term $\eta\left(\boldsymbol{\Phi}_i/k_j\right)$ will pollute the trend that makes the damage still difficult to locate.

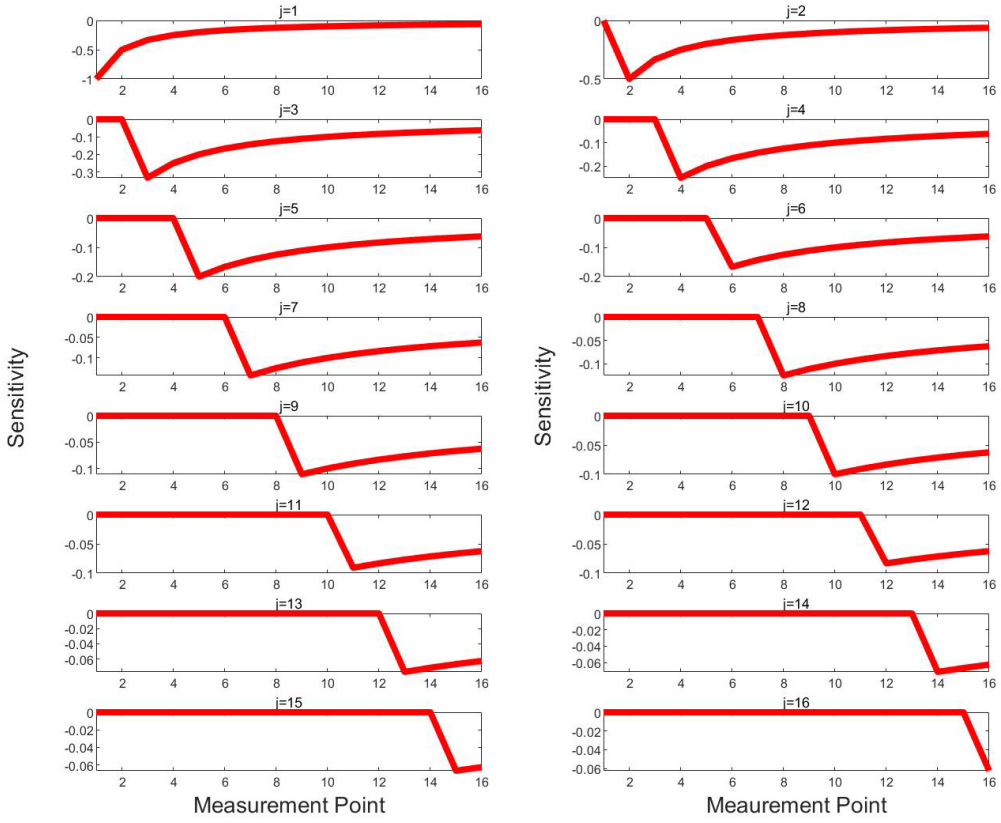

Figure 4 Sensitivity of $\boldsymbol{D}_F$ to the local stiffness k_j, j=1:16.

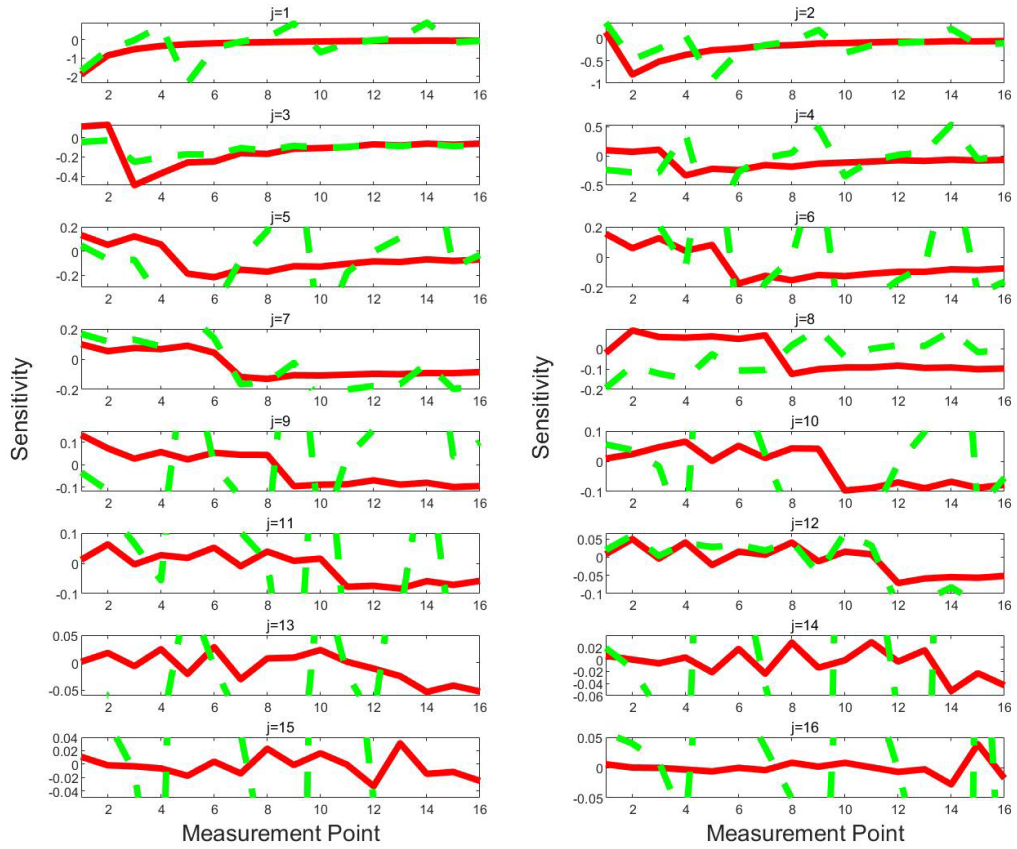

Figure 5 Sensitivity of $\boldsymbol{R}_F^1$ (red solid line) and $\boldsymbol{R}_F^4$ (green dash line) to the local stiffness k_j, j=1:16.

3.3 Damage detection

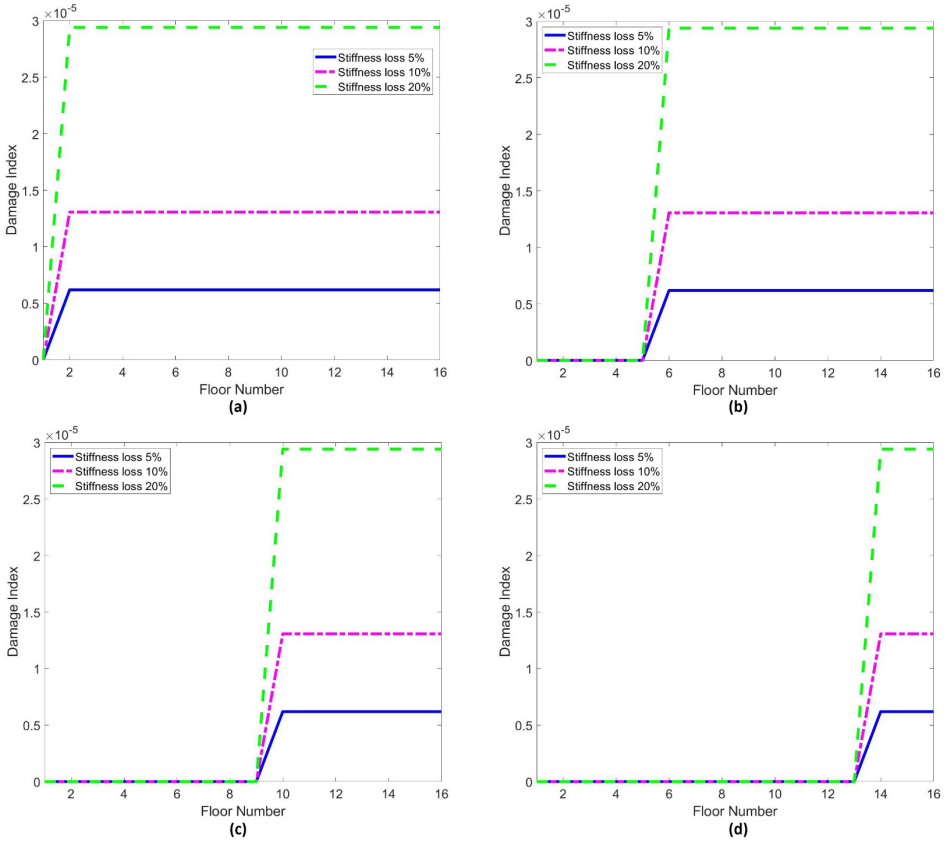

Figure 6 DFV-based damage detection results with damage in (a) Floor Number 2; (b) Floor Number 6; (c) Floor Number 10; (d) Floor Number 14.

Damage with different location (Floor Number 2, 6, 10 and 14) and severity (stiffness loss by 5%, 10% and 20%) is simulated for the 16-story shear frame structure in Figure 1 in this section. The corresponding DFV-based damage index calculated by Eq. (4) using the frequencies and mode shapes of the intact and damaged structure is shown in Figure 6. In all these four subfigures of Figure 6, the blue solid line, the pink dotted line and the green dash-dotted line is the damage index for the stiffness loss by 5%, 10% and 20%, respectively.

In Figure 6, all the damages have been clearly located. Take the blue line in Figure 6b as an example, the blue line in Figure 6b is the damage index when the 6 th floor has a stiffness loss by 5%. Before the 5th floor, the damage index is close to zero. Start from the 6th floor, a sudden change in the damage index is observed. After that, from the 6th to the 12th floor, the damage index remains relatively constant. Therefore, the sudden change location of the damage, the 6th floor, indicates the damage location. In addition, as the stiffness loss becomes larger, the sudden change of the damage index in the 6th floor becomes larger, which shows that this DFV-based damage index can not only located the damage but also show the damage severity. The other subfigures in Figure 6 show the same result.

Furthermore, the damage detection results in Figure 6 coincide well with the sensitivity analysis in Figure 4 in Section 3.2. Again, take the blue line in Figure 6b for example, the corresponding sensitivity analysis result is the 6th subfigure with the title 'j=6' in Figure 4, which is $\eta(\boldsymbol{D}_F/k_6)$. $\eta(\boldsymbol{D}_F/k_6)$ is the sensitivity of $\boldsymbol{D}_F$ to the k_6, which implies how $\boldsymbol{D}_F$ will change when k_6 changes:

From the 6th subfigure in Figure 4, the value of $\eta(\boldsymbol{D}_F/k_6)$ is nearly the same from measurement point 1-5, which means between measurement point 1-5, as 1st-5th floor, this $\boldsymbol{D}_F$ will barely change when k_6 changes.

Then from measurement point 5-6, the value of $\eta(\boldsymbol{D}_F/k_6)$ has a sudden drop to negative, which means between measurement point 5-6, as 5th-6th floor, this $\boldsymbol{D}_F$ will have a sudden increase when k_6 decreases.

After that, from measurement point 6-16, the value of $\eta(\boldsymbol{D}_F/k_6)$ doesn't change much, which means between measurement point 6-16, as 6th-16th floor, this D_F will not change much.

This is just the trend for the blue line in Figure 6b. The other figures between Figure 4 and Figure 6 show the same phenomenon, which explain the reason that this DFV-based damage index can locate the damage.

Figure 7 is the RFV-based damage detection results when 1st row/column of the flexibility matrix is used when the stiffness loss by 5%, 10% and 20% in the 6th floor, respectively. From this figure, the sudden change of the damage index from measurement 5 to 6 can still be detected, so the damage in the 6th floor can still be detected. However, the damage location is not as distinctly identified as in Figure 6b. This also coincide well with the sensitivity analysis result in Figure 5.

Figure 8 is the RFV-based damage detection results when the 4th row/column of the flexibility matrix is used when the stiffness loss by 5%, 10% and 20% in the 6th floor, respectively. In Figure 8, the damage location can not be detected at all. It also coincides with the result from the sensitivity analysis in

In summary, from the DFV/RFV-based damage detection results for the 16-story shear frame structure, the DFV can be used for damage detection. While for RFV, it requires to chose the right row/column number to formulate the damage index, which will be difficult to use in real application.

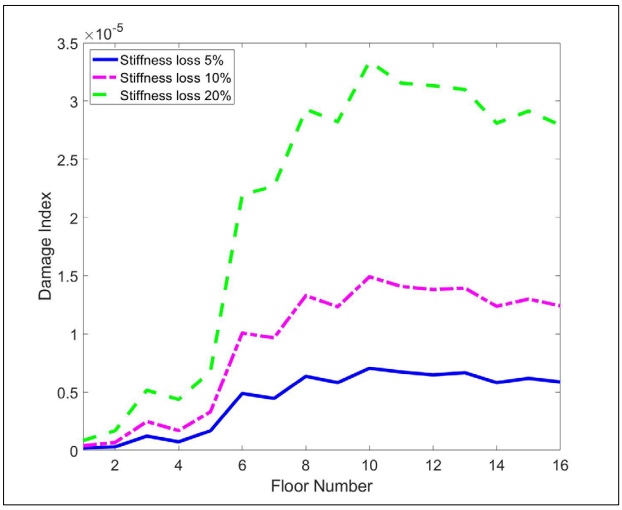

Figure 7 Damage detection result using $\boldsymbol{R}_F^1$.

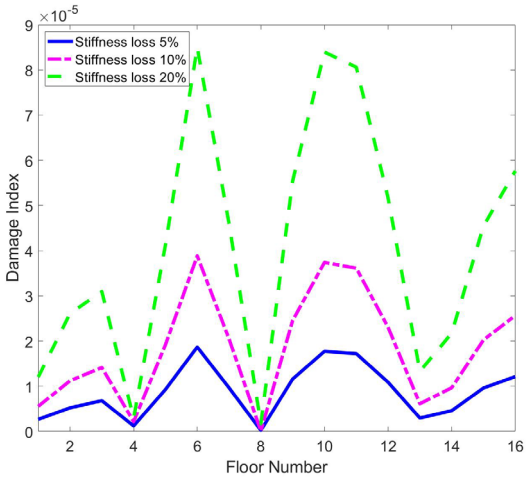

Figure 8 Damage detection result using $\boldsymbol{R}_F^4$.

4 REAL STRUCTURE APPLICATION

In this section, one of the well-known benchmark structures, the I-40 Bridge will be used to verify the DFV/RFV-based damage index. Situated across the Rio Grande River in Albuquerque, New Mexico, USA, the I-40 Bridge is shown in Figure 9a. Further information regarding the bridge and the modal tests is available in Farrar et al. (2000). 26 accelerometers were installed on the bridge, with each side 13 measurements. Four increase levels damages in the same location (DOF 20) were used to simulate the fatigue cracks in the plated-girder bridges, which is named as Damage Case 4-1 - 4-4, respectively. A detailed description of the damage is provided in Farrar et al. (2000), as shown in Figure 9b. The

modal test data can be downloaded from the official website of Los Alamos National Laboratory: https://www.lanl.gov/projects/national-security-education-center/engineering/software/shm-data-sets-and-software.php

The natural frequencies and mode shapes for intact and damaged bridge are shown in Table 1 and Figure 10, respectively. From Table 1, as the modal order increases, the natural frequency of the bridge also increase. But it will decrease when the damage becomes severer from Damage Case 4-1 - 4-4. As shown in Figure 10, the mode shape for the intact and Damage Case 4-1 to 4-3 is nearly the same, while for Damage case 4-4, it has several changes from the other four.

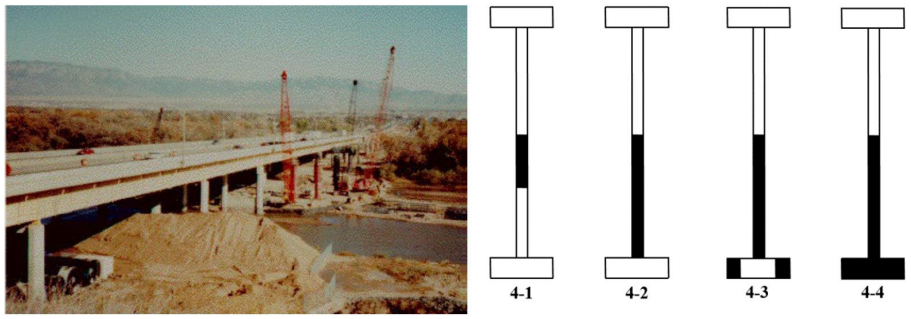

(a) (b)

Figure 9 I-40 Bridge (Farrar et al. 2000): (a) Photo; (b) Four Damage Cases.

Table 1 Natural frequencies of the intact and damaged bridge/Hz

Order	Intact	Damage Case 4-1	Damage Case 4-2	Damage Case 4-3	Damage Case 4-4
1	2.4793	2.5104	2.5207	2.4616	2.2699
2	2.9493	2.9853	2.9907	2.9418	2.8339
3	3.4942	3.5669	3.5139	3.4802	3.4874
4	4.0774	4.1209	4.0950	4.0374	3.9896
5	4.1668	4.2079	4.1953	4.1380	4.1470
6	4.6362	4.6916	4.6638	4.5904	4.5245

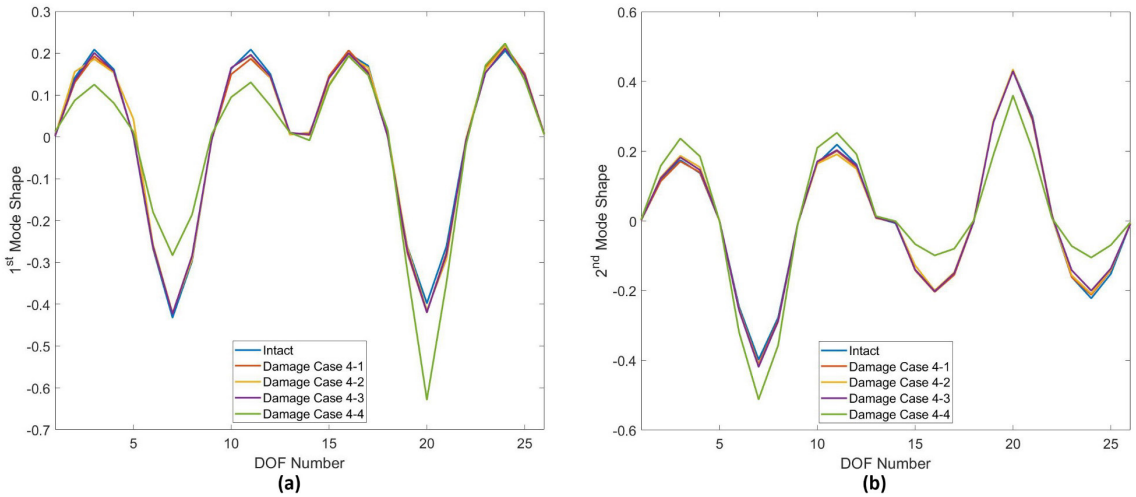

Figure 10 Mode shape: (a) 1st mode shape; (b) 2nd mode shape.

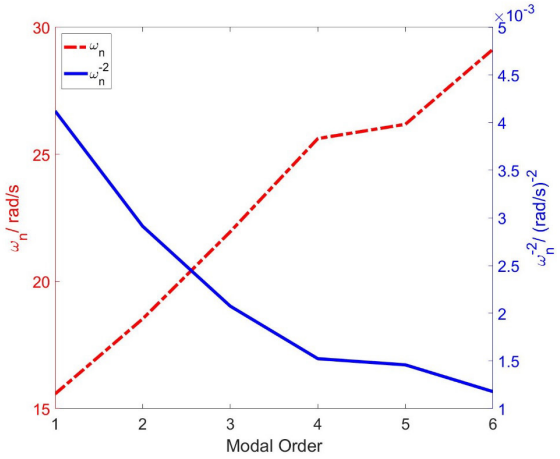

Figure 11 Change of the frequency with the modal order for intact structure.

Figure 11 is the change of the frequency ω_n^i and $(\omega_n^i)^{-2}$ with the modal order for intact structure, we can also see that when the modal order increases, ω_n^i will increase while $(\omega_n^i)^{-2}$ will drop very fast.

Figure 12 is the DFV-based damage index calculated from the modal parameters of the I-40 Bridge using Eq. (4). Figure 12a is the DFV-based damage index calculated using the 6 modes, that there is only one peak value in DOF 20 for the purple line, that is Damage Case 4-4, which correctly locate the damage. The other lines are almost the same that all close to zero. As a result, this DFV-based damage index can locate the damage for Damage Case 4-4 but fails to do so for Damage Case 4-1, 4-2 and 4-3. As shown in Eq. (10) and the numerical simulation, the reason for the DFV can locate the damage is due to the damage-induced-change of the frequency and mode shape. While the damage in the Damage Case 4-1, 4-2 and 4-3 is smaller compare to the damage in Damage Case 4-4, as shown in the frequency in Table. 1 and mode shape in Figure 10, makes this DFV difficult to locate the damage.

Figure 12b shows the similar results that this DFV-based damage index is calculated using just the 1st mode. Although there is a smaller peak value in DOF 7, the damage in Damage Case 4-4 can also be located. This is because the 1st mode shape is sensitive to the damage location and plays an important role in determine the trend of the DFV-based damage index.

Figure 13 is the damage detection results using the 1st row/column of the flexibility matrix, we can see there is a very big peak value of Damage Case 4-4 in DOF 20. As a result, the damage can still be located for this case, this is also because the 1st mode shape is sensitive to the damage location and plays an important part to determine the trend of this RFV-based damage index. Similarly, this RFV-based damage index fails to locate the damage for Damage Case 4-1, 4-2, and 4-3 for the damage is small.

Figure 14 is the damage detection results using the 4th row/column of the flexibility matrix, the damage location couldn't be determined for all the 4 damage cases. This because the 4th mode shape is not sensitive to the damage location, which plays an important part to determine the trend of this RFV-based damage index, the damage could not be detected successfully.

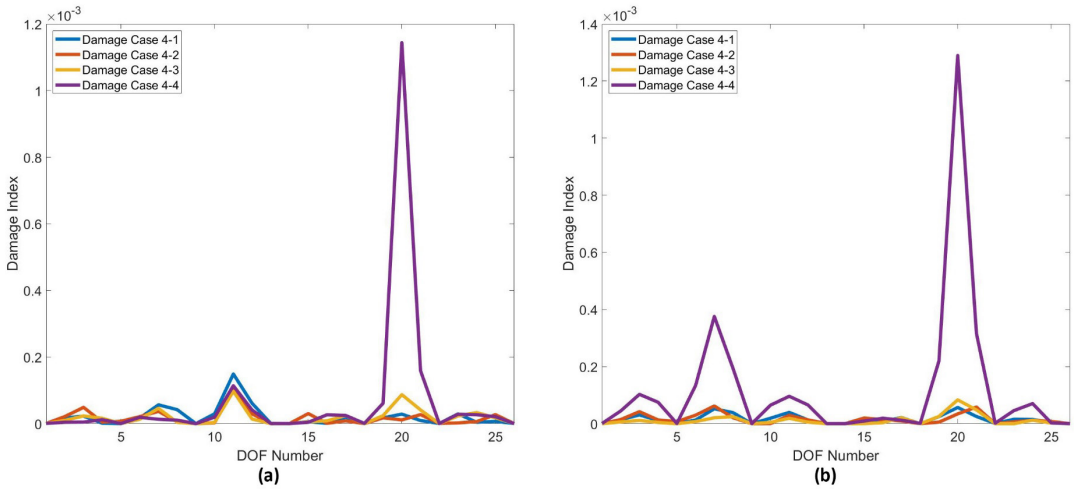

Figure 12 DFV-based damage detection results for different damage cases with:(a) 6 modes; (b) 1st mode.

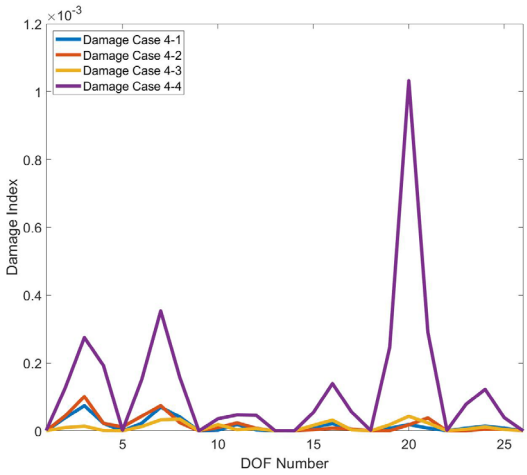

Figure 13 Damage detection results using $\boldsymbol{R}_F^1$.

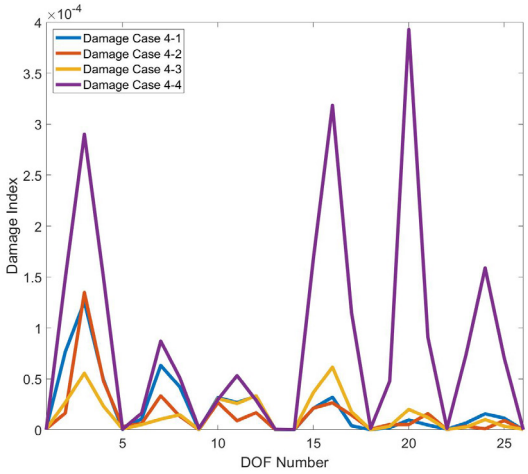

Figure 14 Damage detection results using $\boldsymbol{R}_F^4$.

As a result, this DFV-based damage index can locate the damage using very little modal information when the lower mode shape is sensitive to the damage location. On the other hand, the RFV-based damage index is applicable only when the lower mode shape exhibits sensitivity to the damage location, and the appropriate modal order is selected.

5 CONCLUSIONS

In this paper, the detectability of different parts of the flexibility matrix is studied in detail. Sensitivity analysis is used to show its inherent mechanism for damage localization. It is shown that the Diagonal of Flexibility matrix Vector (DFV) and Row/column of the Flexibility matrix Vector (RFV) defined in this paper is a weighted combination of the Hadamard product of two mode shapes. As the weight is the reciprocal of the square of frequency, as modal order increases, higher mode will contribute very limit to the DFV/RFV. As a result, both DFV/RFV can be obtained using the first few modes. Sensitivity analysis of DFV to the local stiffness shows the DFV will have a sudden change around the stiffness change location, which indicates the DFV can be used for damage localization. This sudden change is contributed by the abrupt change of the sensitivity of the first few mode shapes to the local stiffness. Therefore, the DFV is capable for damage localization when the first few mode shapes are sensitive to the damage location.

While for the RFV, choose the suitable row/column number of the flexibility matrix is a prerequisite, which is corresponding to the modes that the damage affects. But even the right number is selected, which is very difficult in real application, the other mode shapes will still affect the result that makes the RFV very difficult to locate the damage. That's why very limit researchers use one row/column of the flexibility matrix for damage detection.

The well agreement of the results from sensitivity analysis and damage detection of the 16-story shear frame shows DFV is a good indictor not only for damage location but also for damage severity. Moreover, the damage detection result of the I-40 Bridge shows this DFV can be used for real structure. However, how to locate the damage when it is very small in real application, especially for large structure, requires further investigation.

Acknowledgement

The authors are grateful for financial support from the National Natural Science Foundation of China (Grant Nos. 11872190, 11972014), the Natural Science Foundation of Jiangsu Province (Grant Nos. BK 20190834), the Research Start-up Foundation of Jiangsu University (Grant Nos. 19JDG027) and China Scholarship Council (Grant Nos. 202008320084).

Statements and Declarations: The authors declare that they have no known competing financial interests or personal relationships that could have appeared to influence the work reported in this paper.

Author's Contribuitions: Conceptualization, Muyu Zhang and Jianguo Zhu; Methodology, Muyu Zhang and Jian Zhang; Investigation, Xiaoyang Peng, Yujia Li and Ziping Wang; Writing - original draft, Muyu Zhang, Xiaoyang Peng and Yujia Li; Writing - review & editing, Ziping Wang, Jianguo Zhu and Jian Zhang; Funding acquisition, Muyu Zhang, Jianguo Zhu and Jian Zhang; Resources, Ziping Wang and Jianguo Zhu; Supervision, Jianguo Zhu.

Editor: Pablo Andrés Muñoz Rojas

References

An, Y., Błachowski, B., Zhong, Y., Hołobut, P., Ou, J. (2017). Rank-revealing QR decomposition applied to damage localization in truss structures. Structural Control and Health Monitoring, 24(2), e1849.

Avci, O., Abdeljaber, O., Kiranyaz, S., Hussein, M., Gabbouj, M., Inman, D. J. (2021). A review of vibration-based damage detection in civil structures: From traditional methods to Machine Learning and Deep Learning applications. Mechanical Systems and Signal Processing, 147, 107077.

Bernagozzi, G., Quqa, S., Landi, L., Diotallevi, P. P. (2022). Structure-type classification and flexibility-based detection of earthquake-induced damage in full-scale RC buildings. Journal of Civil Structural Health Monitoring, 12(6), 1443-1468.

Bernal, D. (2002). Load vectors for damage localization. Journal of Engineering Mechanics, 128(1), 7-14.

De Medeiros, R., Sartorato, M., Vandepitte, D., Tita, V. (2016). A comparative assessment of different frequency based damage detection in unidirectional composite plates using MFC sensors. Journal of Sound and Vibration, 383, 171-190.

De Medeiros, R., Vandepitte, D., Tita, V. (2018). Structural health monitoring for impact damaged composite: a new methodology based on a combination of techniques. Structural Health Monitoring, 17(2), 185-200.

De Menezes, V. G., Souza, G. S., Vandepitte, D., Tita, V., de Medeiros, R. (2021). Defect and damage detection in filament wound carbon composite cylinders: a new numerical-experimental methodology based on vibrational analyses. Composite Structures, 276, 114548.

Dinh-Cong, D., Nguyen-Huynh, P., Nguyen, S. N., Nguyen-Thoi, T. (2023). Damage identification of functionally graded Beams using Modal Flexibility sensitivity-based damage index. Periodica Polytechnica Civil Engineering, 67(1), 272-281.

Duan, Z., Yan, G., Ou, J., Spencer, B. F. (2005). Damage localization in ambient vibration by constructing proportional flexibility matrix. Journal of Sound and Vibration, 284(1-2), 455-466.

Entezami, A., Sarmadi, H., Saeedi Razavi, B. (2020). An innovative hybrid strategy for structural health monitoring by modal flexibility and clustering methods. Journal of Civil Structural Health Monitoring, 10(5), 845-859.

Farrar, C. R., Cornwell, P. J., Doebling, S. W., Prime, M. B. (2000). Structural health monitoring studies of the Alamosa Canyon and I-40 bridges (No. LA-13635-MS). Los Alamos National Lab.(LANL), Los Alamos, NM (United States).

Gao, Y., Spencer Jr, B. F., Bernal, D. (2004). Experimental verification of the damage locating vector method. Journal of Engineering and Mechanics.

Gharehbaghi, V. R., Noroozinejad Farsangi, E., Noori, M., Yang, T. Y., Li, S., Nguyen, A., Mirjalili, S. (2022). A critical review on structural health monitoring: Definitions, methods, and perspectives. Archives of Computational Methods in Engineering, 29(4), 2209-2235.

Jaishi, B., Ren, W. X. (2006). Damage detection by finite element model updating using modal flexibility residual. Journal of Sound and Vibration, 290(1-2), 369-387.

Jung, H. Y., Sung, S. H., Jung, H. J. (2015). Experimental validation of normalized uniform load surface curvature method for damage localization. Sensors, 15(10), 26315-26330.

Katebi, L., Tehranizadeh, M., Mohammadgholibeyki, N. (2018). A generalized flexibility matrix-based model updating method for damage detection of plane truss and frame structures. Journal of Civil Structural Health Monitoring, 8, 301-314.

Kim, J. T., Ryu, Y. S., Cho, H. M., Stubbs, N. (2003). Damage identification in beam-type structures: frequency-based method vs mode-shape-based method. Engineering Structures, 25(1), 57-67.

Ko, J. M., Sun, Z. G., Ni, Y. Q. (2002). Multi-stage identification scheme for detecting damage in cable-stayed Kap Shui Mun Bridge. Engineering Structures, 24(7), 857-868.

Liu, H., Wu, B., Li, Z. (2021). The generalized flexibility matrix method for structural damage detection with incomplete mode shape data. Inverse Problems in Science and Engineering, 29(12), 2019-2039.

Maia, N. M., Almeida, R. A., Urgueira, A. P., Sampaio, R. P. (2011). Damage detection and quantification using transmissibility. Mechanical Systems and Signal Processing, 25(7), 2475-2483.

Marques, D., Flor, F. R., Medeiros, R. D., Pagani Junior, C. D. C., Tita, V. (2018). Structural health monitoring of sandwich structures based on dynamic analysis. Latin American Journal of Solids and Structures, 15, e58.

Messina, A., Williams, E. J., Contursi, T. (1998). Structural damage detection by a sensitivity and statistical-based method. Journal of Sound and Vibration, 216(5), 791-808.

Mustafa, S., Matsumoto, Y., Yamaguchi, H. (2018). Vibration-based health monitoring of an existing truss bridge using energy-based damping evaluation. Journal of Bridge Engineering, 23(1), 04017114.

Pandey, A. K., Biswas, M. (1995). Experimental verification of flexibility difference method for locating damage in structures. Journal of Sound and Vibration, 184(2), 311-328.

Qiao, P., Lu, K., Lestari, W., Wang, J. (2007). Curvature mode shape-based damage detection in composite laminated plates. Composite Structures, 80(3), 409-428.

Reams, R. (1999). Hadamard inverses, square roots and products of almost semidefinite matrices. Linear Algebra and its Applications, 288, 35-43.

Sartorato, M., De Medeiros, R., Vandepitte, D., Tita, V. (2017). Computational model for supporting SHM systems design: Damage identification via numerical analyses. Mechanical Systems and Signal Processing, 84, 445-461.

Sohn, H., Farrar, C. R., Hemez, F. M., Shunk, D. D., Stinemates, D. W., Nadler, B. R., Czarnecki, J. J. (2003). A review of structural health monitoring literature: 1996-2001. Los Alamos National Laboratory, USA, 1, 16.

Styan, G. P. (1973). Hadamard products and multivariate statistical analysis. Linear Algebra and its Applications, 6, 217-240.

Sun, Y., Yang, Q., Peng, X. (2022). Structural Damage Assessment Using Multiple-Stage Dynamic Flexibility Analysis. Aerospace, 9(6), 295.

Wang, J., Qiao, P. (2007). Improved damage detection for beam-type structures using a uniform load surface. Structural Health Monitoring, 6(2), 99-110.

Wang, L., Yang, Z., Waters, T. P. (2010). Structural damage detection using cross correlation functions of vibration response. Journal of Sound and Vibration, 329(24), 5070-5086.

Wu, D., Law, S. S. (2005). Sensitivity of uniform load surface curvature for damage identification in plate structures. Journal of Vibration and Acoustics, 127(1), 84-92.

Yang, S., Huang, Y. (2021). Damage identification method of prestressed concrete beam bridge based on convolutional neural network. Neural Computing and Applications, 33(2), 535-545.

Zhang, C., Mousavi, A. A., Masri, S. F., Gholipour, G., Yan, K., Li, X. (2022). Vibration feature extraction using signal processing techniques for structural health monitoring: A review. Mechanical Systems and Signal Processing, 177, 109175.

Zhang, J., Xu, J. C., Guo, S. L., Wu, Z. S. (2013). Flexibility-based structural damage detection with unknown mass for IASC-ASCE benchmark studies. Engineering Structures, 48, 486-496.

Zhang, M.Y., Li, Y.J., Peng, X.Y., Wang, Z.P., Zhu, J.G. (2023). Damage assessment using the auto-correlation-function-based damage index. International Journal of Acoustics and Vibration, 28(3), 239-248.

Zhang, Z., Aktan, A. E. (1995). The damage indices for the constructed facilities. In Proceedings-SPIE the international society for optical engineering (pp. 1520-1520). SPIE International Society for Optical.

Zhao, J., DeWolf, J. T. (1999). Sensitivity study for vibrational parameters used in damage detection. Journal of Structural Engineering, 125(4), 410-416.